JOURNAL OF GEOPHYSICAL RESEARCH: BIOGEOSCIENCES, VOL. 118, 1660–1673, doi:10.1002/2013JG002408, 2013

Sierra San Pedro Mártir, Baja California, cool-season precipitation reconstructed from earlywood width of *Abies concolor* tree rings

D. M. Meko,[1] R. Touchan,[1] J. Villanueva Díaz,[2] D. Griffin,[1,3] C. A. Woodhouse,[1,3] C. L. Castro,[4] C. Carillo,[4] and S. W. Leavitt[1]

Received 1 June 2013; revised 7 November 2013; accepted 12 November 2013; published 10 December 2013.

[1] Tree ring data are analyzed for a multicentury record of drought history in the Sierra San Pedro Mártir (SSPM) of Baja California, Mexico. Climatic variation in the study area is of particular interest because the SSPM is a rich biotic environment at the southern limit of the California floristic province and the southern limit of the planetary jet stream. Future shifts in the jet stream would be expected to have amplified effect on this marginal environment. The study applies linear regression to tree ring indices of earlywood-width of *Abies concolor* to estimate a 353 year (1658–2010 C.E.) record of cool-season (October–April) precipitation, *P*, in SSPM. Time-nested regression models account for more than half the variance of grid point *P* in calibration periods of length 50–65 years. Cross-spectral analysis indicates strong tracking of observed *P* by the reconstruction over a broad range of frequencies. Robustness of the reconstruction is supported by synchrony of reconstructed *P* with tree ring variations in other tree species from SSPM. The reconstruction emphasizes the severity of the 1950s drought in a long-term context and the single-year intensity of droughts in the last decade: 2007 stands out as the driest reconstructed year, with a high percentage of missing rings in *A. concolor*. The reconstruction identifies the early twentieth century pluvial as the wettest epoch in the last 353 years in the SSPM. High-elevation tree species in SSPM may be especially well-suited to sensing snowpack-related moisture variations associated with a southerly branched jet stream and the types of weather systems active in the pluvial.

Citation: Meko, D. M., R. Touchan, J. Villanueva Díaz, D. Griffin, C. A. Woodhouse, C. L. Castro, C. Carillo, and S. W. Leavitt (2013), Sierra San Pedro Mártir, Baja California, cool-season precipitation reconstructed from earlywood width of *Abies concolor* tree rings, *J. Geophys. Res. Biogeosci.*, *118*, 1660–1673, doi:10.1002/2013JG002408.

1. Introduction

[2] The Sierra San Pedro Mártir (SSPM), a rugged granitic range with highest elevations over 3000 m in the northern part of the Peninsula of Baja California, Mexico, is directly exposed to weather systems delivering precipitation to northern Mexico and the southwestern United States. The Sierra is influenced by cyclones embedded in southward excursions of the jet stream, cutoff low pressure systems, occasional northward meandering of Pacific tropical storms, and westward extensions of summer moisture from the North American Monsoon [*Hastings and Turner*, 1965; *Markham*, 1972; *Pike*, 1972]. Precipitation variability in the winter is strongly linked to El Niño–Southern Oscillation (ENSO) and to positioning of ridges and troughs in the westerlies over the North Pacific Ocean and western North America [*Minnich et al.*, 2000].

[3] The Sierra forms the southern limit of the Californian floristic province, an important center of biodiversity threatened by accelerating development [*Minnich et al.*, 1997]. Located at the equatorward margin of the planetary jet stream, the Sierra may be especially sensitive to future climate change, as one expected effect of global warming is a northward shift of the jet stream and main belt of the westerlies [e.g., *Shindell et al.*, 1999; *Lu et al.*, 2008].

[4] Planning for management of natural resources in the face of climate change can benefit from improved knowledge of local and regional climate variability on time scales of decades to centuries. While the precipitation record at Ensenada, on the west coast of Baja, begins in 1894 [*Hastings and Turner*, 1965], records in the mountains are generally short and often discontinuous [*Minnich et al.*, 2000; *Álvarez et al.*, 2007]. Tree ring records have been widely applied for extension of precipitation records in the

Additional supporting information may be found in the online version of this article.

[1]Laboratory of Tree-Ring Research, University of Arizona, Tucson, Arizona, USA.
[2]Laboratorio de Dendrocronologia, Instituto Nacional de Investigaciones Forestales, Agricolas, y Pecuarias, Gomez Palacio, Mexico.
[3]School of Geography and Development, University of Arizona, Tucson, Arizona, USA.
[4]Department of Atmospheric Sciences, University of Arizona, Tucson, Arizona, USA.

Corresponding author: D. M. Meko, Laboratory of Tree-Ring Research, University of Arizona, 1215 E. Lowell St., Tucson, AZ 85721, USA. (dmeko@LTRR.arizona.edu)

2169-8953/13/10.1002/2013JG002408

southwestern United States [e.g., *Ni et al.*, 2002; *Salzer and Kipfmueller*, 2005; *Touchan et al.*, 2011; *Griffin et al.*, 2013]. Tree ring studies have effectively addressed variability of precipitation at long time scales in parts of Mexico [e.g., *Cleaveland et al.*, 2003; *Diaz et al.*, 2002], including Baja California Sur [*Diaz et al.*, 2001], but no precipitation reconstruction has yet been published for the SSPM.

[5] The Sierra contains stands of several dendroclimatologically useful North American tree species near the southern edge of their North American range. These species include *Abies concolor* (white fir) and *Pinus lambertiana* (sugar pine) [*Little*, 1971]. The dendroclimatological potential in the Sierra is well demonstrated. The International Tree Ring Data Bank (ITRDB) includes *Pinus jeffreyi* (Jeffrey pine) chronologies from collections in 1972 and 1995 (http://www.ncdc.noaa.gov/paleo/treering.html). A reconstruction of the Pacific Decadal Oscillation by *Biondi et al.* [2001] includes a *P. jeffreyi* chronology from SSPM in the predictor tree ring network. Unpublished tree ring chronologies of *P. jeffreyi*, *P. lambertiana*, and *A. concolor* collected by the primary author in 1994 and 1995 are part of the network of tree ring predictors for the North America Drought Atlas [*Cook et al.*, 2004, 2007].

[6] In this paper, we apply earlywood-width measurements of *A. concolor* tree rings updated by collections in 2010 to study precipitation variability in SSPM over the past several centuries. A reconstruction of cool-season precipitation to 1658 C.E. is derived by time-nested regression and is analyzed to place recent droughts and wet periods in a long-term perspective. Exceptionally wet or dry years are examined for a statistical link with indices of ocean/atmosphere behavior. The possible relevance of temperature trend to interpretation of the reconstruction is addressed with correlation and trend analysis.

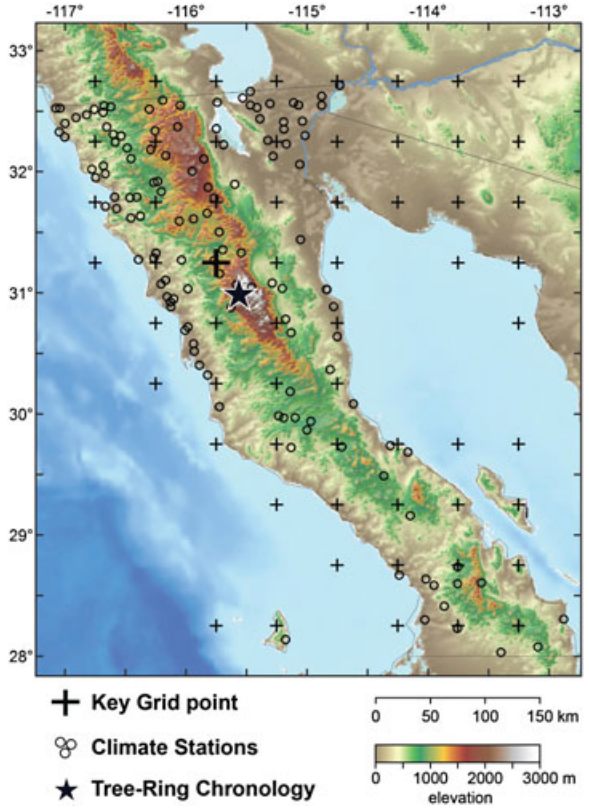

Figure 1. Map showing locations of tree ring site, climatic stations, and climate grid points. Tree ring site marked by triangle, climate stations (132 total) by small circles, and 0.5° climate-data grid points (see text) by plus signs. Grid point nearest the tree ring site enlarged.

2. Study Area and Data

[7] The SSPM is a fault-bounded range that extends southeastward over a distance of 145 km on the Baja California peninsula and forms part of the drainage divide between the Pacific Ocean and the Gulf of California (Figure 1). At the spine of the range at its northern end is a plateau at an elevation of about 2400 m. The plateau is bounded on the west by a smooth undissected escarpment with local relief of 300–600 m and on the east by peaks as high as 3100 m and a highly dissected escarpment dropping steeply down to the floor of the Sonoran Desert, at an elevation of 500 m [*Minnich et al.*, 1997].

[8] The wood samples for this study are increment cores of *A. concolor* from merged field collections in 1995 and 2010 from the north slope of Cerro del la Cúpula (31.00°N, 115°W, 2720 m.a.s.l.), at the eastern edge of the plateau, and from the western edge of the plateau near the entrance to Sierra de San Pedro Mártir National Park (31.05°N, 115.47°W, 2440 m.a.s.l.) The full collection consists of cores from 43 trees—25 from the upper subsite and 18 from the lower. The collection trips in 1995 and 2010 also included sampling of *P. jeffreyi* and *P. lambertiana*, whose chronologies are used in a peripheral way in this paper.

[9] Tree ring samples were prepared, and width of rings were cross-dated and measured according to standard procedures [*Stokes and Smiley*, 1996]. The collections in 2010 are part of a larger study of the North American Monsoon (NAM) using subannual (earlywood and latewood) chronologies of conifer tree ring width. The merged set of cores from the 1995 and 2010 collections were processed according to the uniform protocol of the NAM study [*Griffin et al.*, 2011]. This protocol includes detrending of each measured series with a cubic smoothing spline [*Cook and Peters*, 1981] with frequency response of 0.50 at a wavelength of 70% of the series length. From exploratory correlation analysis of precipitation with indices of total width, latewood width, and earlywood width, we choose the standard index [*Cook*, 1985] of earlywood width for this study.

[10] The standard site chronology is computed as the median of core indices if fewer than six cores are present and otherwise as the biweight mean [*Cook*, 1985]. While the earliest measured ring of the *A. concolor* collection is 1610, we truncate the period for precipitation reconstruction to begin in 1658, when the sample size reaches three trees and a site chronology averaged over cores has an expressed population signal statistic exceeding the recommended threshold of 0.85 [*Wigley et al.*, 1984].

[11] Precipitation and temperature data are used to identify the seasonal climatic signal in tree rings and to calibrate reconstructions models. Precipitation data for these analyses are from a monthly 0.5° gridded dataset for North America developed by Russ Vose and Richard Heim of the U.S. National Oceanic and Atmospheric Administration

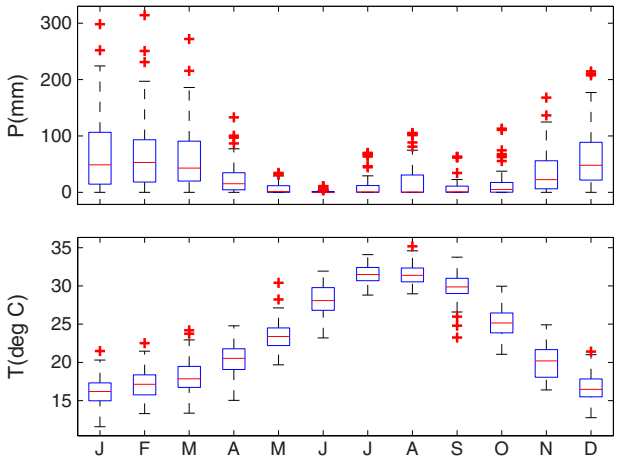

Figure 2. Climograph summary of gridded monthly precipitation and mean maximum daily temperature at 31.25°N, 115.75°W. Analysis period 1946–2010.

(NOAA). Temperature data are from a 0.5° gridded data set of monthly averages of daily maximum temperature developed by the University of Delaware [*Willmott and Matsuura*, 1995; *Willmott and Robeson*, 1995] (http://climate.geog.udel.edu/~climate/html_pages/archive.html). Both gridded data sets utilize interpolation assisted by digital elevation models and are described in more detail in a recent application to regional climate model verification [*Castro et al.*, 2012]. We define the grid point nearest the tree ring site, 31.25°N, 115.75°W, as the "key grid point" (Figure 1) for calibration of reconstruction models and for other diagnostic climatic analyses.

[12] Station monthly precipitation and mean temperature data for 132 stations in Baja California were obtained from Dr. Arthur Douglas; these station data are used primarily to identify the period when station coverage likely becomes adequate to render the gridded P-NOAA precipitation representative of the high mountains of SSPM.

[13] Data downloaded from the International Tree Ring Data Bank (ITRDB) to check consistency of reconstructed precipitation with other tree ring-derived paleoclimatic series include *P. jeffreyi* chronology mexi020 [*Biondi et al.*, 2001] and a precipitation reconstruction for Durango, Mexico [*Cleaveland et al.*, 2003]. A precipitation reconstruction for Baja California Sur [*Diaz et al.*, 2001] and a time series of reconstructed standardized precipitation index for North American Monsoon region 2 [*Griffin et al.*, 2013] are also used in the consistency check.

[14] Two indices of large-scale ocean-atmosphere anomalies were downloaded from NOAA's Earth System Research Laboratory (http://www.esrl.noaa.gov/psd/data/climateindices/): monthly Niño3.4 index, a measure of sea surface temperature (SST) anomaly in the east-central equatorial Pacific; and monthly rank time series of the Extended Multivariate ENSO Index, which incorporates information from SST, sea level pressure, and other variables [*Wolter and Timlin*, 2011]. Additional indices of atmospheric circulation anomaly were downloaded from the National Weather Service Climate Prediction Center (http://www.cpc.ncep.noaa.gov/products/precip/CWlink/pna/pna_index.html). These include monthly indices of the Pacific/North America pattern (PNA) and the Tropical/Northern Hemisphere pattern (TNH)—teleconnection patterns in upper air geopotential height anomalies reflecting jet stream positioning over North America [*Barnston and Livezey*, 1987]—and of the Arctic Oscillation, which reflects the pressure difference between the polar regions and the midlatitudes and is related to the prevalence of zonal versus meridional flow and the penetration of arctic air to southerly latitudes [*Mo and Livezey*, 1986; *Thompson and Wallace*, 1998].

[15] The climate of SSPM as summarized by the gridded climate data is Mediterranean, with dry summers and wet winters, but with a hint of a secondary precipitation peak in August (Figure 2). Cool-season precipitation at the key grid point is correlated highest with precipitation at other grid points on the western side of the mountain axis of Baja California, while correlations greater than 0.8 occur toward the north and north-northeast into southern California and central Arizona (Figure 3). In contrast, correlation drops off rapidly to the south and falls below 0.2 for even the northern parts of Baja California Sur.

[16] Long-term continuous precipitation records are lacking from the Sierra, but a series of bulk precipitation gages in operation for several years after 1990 indicate that mean annual precipitation ranges from about 270 mm at the western base of the Sierra to 600 mm on the western plateau [*Minnich et al.*, 1997]. Mean annual gridded precipitation at the key grid point is 392 mm for 1946–2010. Winter is the dominant season of precipitation on the plateau, with as much as 80% of the winter total falling as snow [*Minnich et al.*, 1997].

3. Methods

3.1. Reconstruction

[17] The seasonal climatic signal in the standard site chronology is summarized with program `seascorr`, which utilizes monthly precipitation and temperature data and measures the strength of correlation between tree rings and the climate signal integrated over seasons of variable length

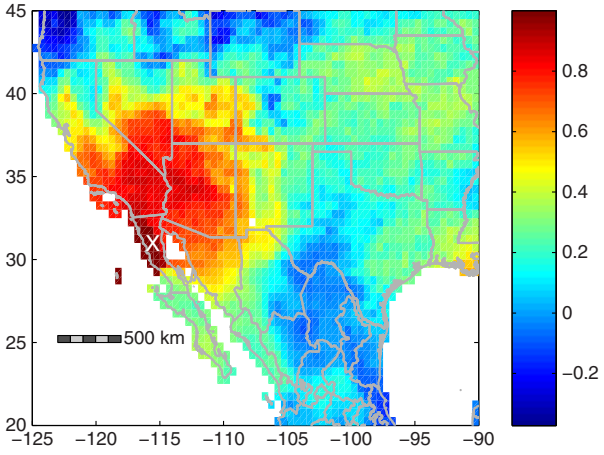

Figure 3. Spatial correlation pattern of gridded cool-season (October–April) precipitation at 31.25°N, 115.75°W. Tree ring site marked by white "X." Analysis period 1946–2010.

[*Meko et al.*, 2011]. From a survey of time coverage by station precipitation data (see Figure S1 in the supporting information), we restricted the `seascorr` analysis to the period 1946–2010 and also adopted that period as a calibration period for the reconstruction. A start year of 1946 allows 65 years for the `seascorr` summary and 50 years (1946–1995) for calibration of reconstruction models with tree ring data collected in 1995 (see below).

[18] The reconstruction model is simple linear regression [*Weisberg*, 1985] of log-transformed seasonal-total precipitation, P on the tree ring index. Transformation was necessary to avoid severe violation of regression assumptions on normality of errors and homogeneity of error variance. The reconstruction approach used here is time-nested modeling applied at the level of the site chronology [*Meko*, 1997]. In this approach, constant-sample (same cores) subchronologies are built to ensure that the calibration and reconstruction segments for a nested model are comprised of the identical cores. The starting point is the time series matrix ${}_m\mathbf{X}_n$ of core indices for n cores and m years. Matrix $\mathbf{X}$ is typically increasingly populated with missing values toward the early years because there are fewer old trees than young trees at the site. Let $I = \{1, \ldots, m\}$ be the set of row numbers and $J = \{1, \ldots, n\}$ be the set of column numbers in $\mathbf{X}$.

[19] Specify k target years of the tree ring record to define constant-sample chronology subsets for nested reconstruction models. The target years are arbitrary but are chosen to represent periods with relatively large differences in sample size or number of cores. To be included in a chronology subset, cores must be present in the target year and extend over succeeding years including all years of a desired minimum-length calibration period. Let $\{H_j \in J, j = 1, \ldots, k\}$ be the sets of columns of $\mathbf{X}$ for the subsets and $\{L_j \in I, j = 1, \ldots, k\}$ be the corresponding rows (years) of $\mathbf{X}$ with no missing data at any cores in the subsets. Core indices for each subset are averaged over cores to form alternative constant-sample site chronologies. The years in set L_j define the potential period for reconstruction by the jth constant-sample subchronology.

[20] The next step in the nested modeling is repeated application of linear regression to calibrate regression equations for each of the k subset chronologies. The result is a set of k reconstruction equations:

$$\hat{y}_{t,j} = \hat{b}_{0,j} + \hat{b}_{1,j} x_{t,j} \tag{1}$$

where $\hat{y}$ is the predicted climate variable, x_t is the predictor or tree ring index, $\hat{b}_0$ and $\hat{b}_1$ are the estimated regression constant and slope coefficient, and subscripts t and j refer to year and subperiod model. Each model has its own regression residuals,

$$\hat{e}_{t,j} = y_t - \hat{y}_{t,j} \tag{2}$$

computed over the calibration period of the jth model.

[21] Each model is then applied to generate a segment of reconstruction, marked by row indices L_j of $\mathbf{X}$, and the individual segments are spliced together into a single final reconstructed time series. The final reconstruction is built by merging the individual nested-model reconstructions, with the reconstructed value for any given year provided by the nested model with highest regression R^2.

[22] Residuals of individual nested models are checked graphically for evidence of violation of regression assumptions on normality, autocorrelation, and relationship to fitted values (predictions) [*Weisberg*, 1985]. The graphical check is supplemented by a Durbin-Watson test for significant lag-1 autocorrelation [*Weisberg*, 1985] and a Lilliefors test for normality [*Conover*, 1980]. Possible trend in residuals is assessed from the significance of the slope coefficient in a regression of residuals on time.

[23] The nested models are validated by cross-validation [*Michaelsen*, 1987], and validation skill is measured by the reduction-of-error statistic [*Fritts et al.*, 1990]. A confidence interval for reconstructed P is estimated by the Monte Carlo approach of noise-added reconstructions [e.g., *Touchan et al.*, 1999; *Meko et al.*, 2001]. This approach consists of generating an ensemble of many (e.g., 1000) plausible time series of observed P by adding sampled random-normal noise with mean zero and variance equal to the variance of the cross-validation regression residuals to the reconstruction. The empirical distribution of noise-added reconstructions each year provides the desired confidence interval (e.g., 25th and 75th percentile for a 50% confidence interval). Confidence intervals for smoothed versions of the reconstruction were derived similarly from the empirical distribution of smoothed noise-added series. A step-by-step summary of the reconstruction procedure is provided in the supporting information.

3.2. Analysis of Reconstructions

[24] Analyses address model validation, occurrence of droughts and wet periods, temperature interactions, and large-scale climatic factors. Agreement of reconstructed and observed P as a function of frequency is summarized by cross-spectral analysis [*Stockton and Meko*, 1983]. Cross spectra are estimated by the smoothed periodogram method [*Bloomfield*, 2000], following the steps listed in *Meko et al.* [2012].

[25] The statistical significance of linear relationships between pairs of time series is checked with the product-moment correlation coefficient [*Wilks*, 1995], after possible adjustment for loss of degrees of freedom due to autocorrelation [*Dawdy and Matalas*, 1964]. Such adjustment is applied only if a one-sided t test [*Haan*, 2002] indicates that both series are significantly ($\alpha = 0.05$) positively autocorrelated at a lag of 1 year.

[26] Smoothed time series variations are described using Gaussian filters with a frequency response of 0.5 at wavelengths $\lambda = 5.2$, 10.2, and 25 years. Filters were designed following *Mitchell et al.* [1966]; weights are listed in the supporting information.

[27] Temperature influence on tree ring series used for the precipitation reconstruction is evaluated in three ways, all aimed at detecting *independent* influence of temperature. "Independent" in this context is over and above the influence inherent in any covariation of temperature with precipitation. First is a check of partial correlations [*Panofsky and Brier*, 1968] of tree ring series with temperature when both variables are controlled for influence of precipitation. This analysis is part of the output of program `seascorr` [*Meko et al.*, 2011]. Second is a check for correlation of temperature with residuals of the regression model used to reconstruct precipitation from the tree ring series. Third is a check for trend (either opposing or same direction) in both temperature and the regression residuals.

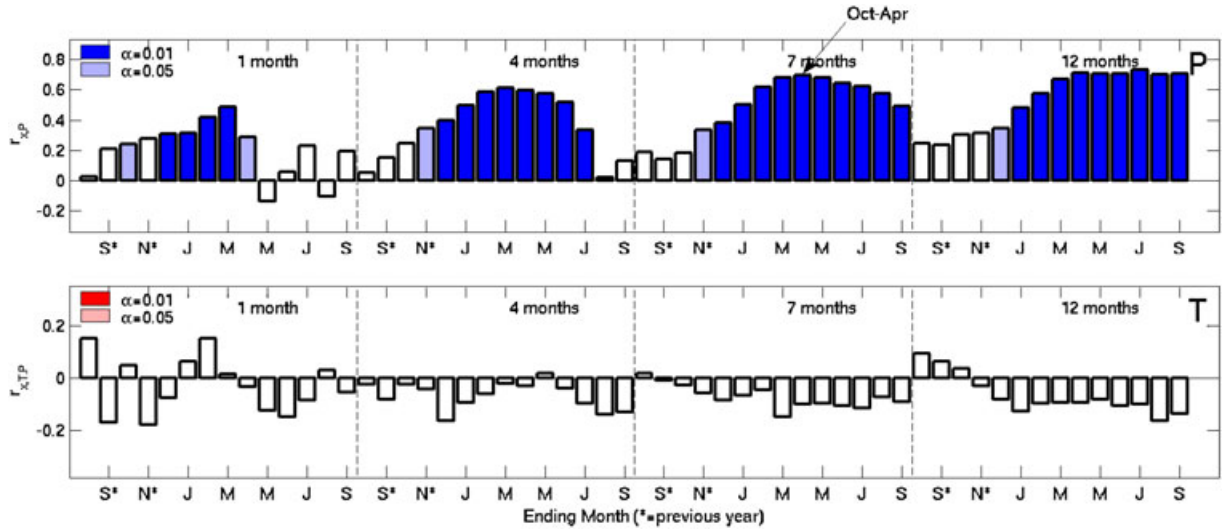

Figure 4. Program `seascorr` summary of seasonal climatic signal in *Abies c.* standard chronology of earlywood width. (top) Correlations for precipitation. (bottom) Partial correlations for temperature. Bars are proportional to correlations and partial correlations for 14 individual months ending with September of growth year (leftmost bars) and for monthly groupings of 4, 7, and 12 months ending in those 14 months. Precipitation is sum over months, and temperature is mean of daily maximum. Peak 7 month grouping is annotated. Analysis period 1946–2010.

[28] Association of dry or wet years (observed and reconstructed) in SSPM with large-scale features of ocean-atmosphere variability is examined graphically with bubble plots. These plots are essentially scatterplots of one climate index on another (e.g., PNA on Niño 3.4) with symbols coded according to sign and magnitude of precipitation anomaly.

4. Results and Discussion

4.1. Reconstruction Modeling

[29] The standard tree ring site chronology is positively correlated with precipitation in most months of the year over the 65 year period 1946–2010 (Figure 4). Correlations for individual months are highest for October of the year preceding growth through April of the growth year. Correlations increase as precipitation is summed over longer monthly groupings; the highest-correlated 7 month and 12 month groupings are October–April (r = 0.70) and August–July (r = 0.73). Partial correlations between tree ring index and temperature, plotted in the bottom of Figure 4, are not significant, indicating that temperature has no independent influence on growth beyond that explainable by intercorrelation of temperature with precipitation. Correlations of monthly temperature with precipitation (not shown) for the same analysis period are negative for 11 of the 12 months of the year and exceed –0.4 for the block of cool-season months December–April.

[30] Four regression models, with R^2 ranging from 0.50 to 0.52, were used in the time-nested reconstruction of cool-season (October–April) precipitation, P (Table 1). The reconstruction segment supplied by any of these models is based on a constant-sample (same cores) chronology. The sample size varies greatly among models, from just four cores for the earliest nest to the 69 cores for the penultimate nest. The drop to 51 cores for the last nest reflects the loss of cores from the 1995 collection. All models have skill of validation (positive RE) and show little dropoff from calibration R^2 to validation RE.

[31] Regression R^2 is stable across nested models despite the great differences in sample size of the subchronologies

Table 1. Statistics of Reconstruction Models[a]

	Calibration[c]				Validation[d]		Reconstruction[e]		
Model[b]	Years	b_0	b_1	R^2	RE	s_e	N	Full	Contributed
M1658	1946–1995	2.186	0.319	0.496	0.46	0.1496	4	1658–1995	1658–1749
M1750	1946–1995	2.163	0.347	0.515	0.48	0.1464	28	1750–1995	1750–1847
M1848	1946–1995	2.134	0.374	0.518	0.48	0.1459	69	1848–1995	1848–1995
M1996	1946–2010	2.104	0.397	0.515	0.49	0.1516	51	1914–2010	1996–2010

[a]Statistics apply to models with log-transformed precipitation as predictor.
[b]Models coded by first year contributed to blended reconstruction.
[c]Calibration period (Years), regression constant (b_0), regression coefficient end (b_1), and coefficient of determination (R^2).
[d]Reduction-of-error statistic (RE) and standard deviation of cross-validation residuals (s_e).
[e]Number of cores (N) averaged to form site chronology for the "Full" reconstruction period, start and end years of the "Full" period possible to be reconstructed with the model, and start and end years of segment contributed by the model to the final reconstruction.

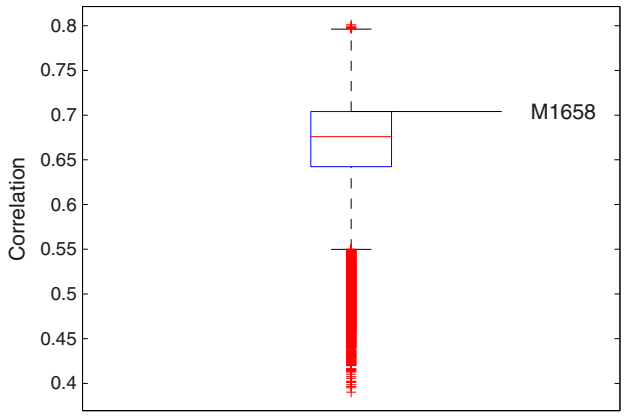

Figure 5. Distribution of correlation coefficients of log-transformed annual *P*, 1946–1995, with all possible chronologies built from unique four-core subsets of 79 cores representing the period 1946–1995. Each chronology is computed as the median of the four-core indices. Correlation for the model M1658 (r = 0.70) is annotated. Boxplot represents 1,502,501 correlations with range 0.39–0.80 and median (horizontal line in box) of 0.68.

(Table 1). The sensitivity of the precipitation signal of the poorest replicated model (M1658) to the makeup of the subchronology was tested by repeating the regression modeling for all sets of four-core chronologies possible from unique combinations of the 79 cores that span the period 1946–1995. Model M1658 happens to be one of more than 1.5 million such combinations. The R^2 for the set of cores in M1658 is at the 75th percentile of sample R^2 (Figure 5). This high ranking attests to the relative strength of precipitation signal in those oldest trees at the site. The wide distribution of R^2, however, underscores the risk of a small-sample chronology. For example, the weakest quartile of four-core subchronologies has correlation with *P* of $r < 0.64$, corresponding to $R^2 < 0.41$, while the weakest single combination has $r = 0.39$, or $R^2 = 0.15$.

[32] Analysis of residuals for the four nested reconstruction models shows no violations of regression assumptions. Histograms of residuals shows no strong departure from normality, Durbin-Watson statistics are not statistically significant, and no patterns are apparent in plots of residuals on fitted values. Diagnostic plots for analysis of residuals for the individual nested regression model are provided in Figures S2–S5 of the supporting information.

[33] Reconstructed *P* closely tracks the observed *P* over the 1946–2010 calibration period (Figure 6a). Reconstruction errors are relatively large, with a distinct tendency to underestimate wetness, in wet years (e.g., 1978–1980). This bias and a corresponding but less obvious bias to underestimate the severity of negative *P* departure in dry years are a consequence of the least squares regression procedure, which tends to produce "conservative" estimates (i.e., compressed toward the calibration mean relative to the observed predictand). The tendency is illustrated in a scatter of reconstructed on observed *P*: The axis of the scatter of points is horizontally oriented relative to the 1:1 line of a theoretical perfect reconstruction (red dashed) (Figure 6b). Log transformation of the predictand further amplifies the bias on the wet side when predictions are back transformed to original precipitation units (Figure 6c).

[34] Spectral analysis for the 1946–2010 calibration period shows that observed *P* differs from white noise significantly only at highest frequencies, where variance is lower than expected (Figure 7a). The proportion of the variance at low frequencies is slightly greater for reconstructed *P* than for observed *P* during this common period (Figures 7a and 7b), perhaps reflecting some bias due to use of standard rather than residual chronologies. The reconstruction is strongly coherent with observed *P* except at highest frequencies and other parts of the frequency range where variance of observed *P* is low (Figure 7c). Where coherence is high, the two series are generally in phase (Figure 7d). The exception is near a wavelength of 15 years (frequency 0.07), where the phase difference of 50° corresponds roughly to an small offset of about 2 years. While suggesting a tendency to overestimate persistence of departures (e.g., drought duration), the spectral, coherency and phase plots broadly support the ability of the reconstruction to track decadal to multidecadal variations in *P*.

4.2. Long-Term Reconstruction

[35] The final reconstruction assembled by prioritizing and splicing the individual nested reconstructions covers 1658–2010 and exhibits large fluctuations year-to-year as well as on wavelengths of multiple decades (Figure 8). The longest wavelike feature is the swing from a high in the mid-1910s to a low in the 1950s and back to a high in the 1980s. In the late 1990s, the reconstruction again begins to decline. The 1910s–1980s wave contains the single-year high (1918) in the 353 year reconstruction, and the most

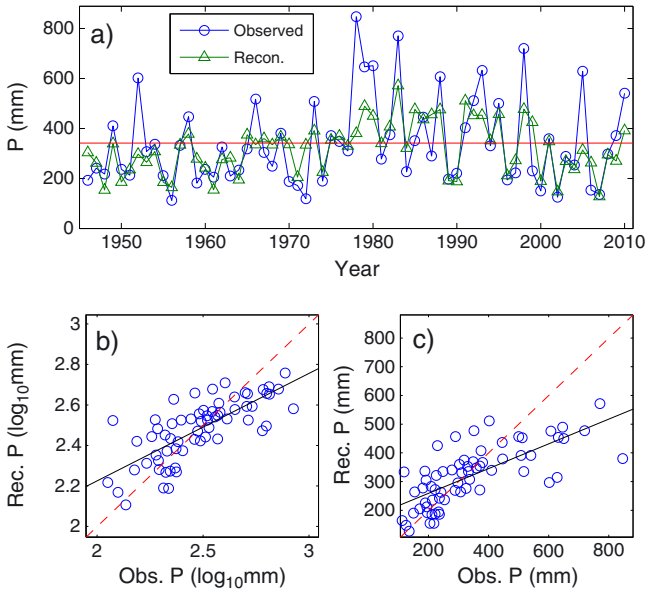

Figure 6. Agreement of reconstructed with observed precipitation. (a) Time plots, (b) scatterplot of log-transformed precipitation, and (c) scatterplot of precipitation in units of millimeter. Horizontal line in Figure 6a at calibration period (1946–2010) is the observed mean. Dashed lines in Figures 6b and 6c represent perfect agreement between reconstructed and observed precipitation.

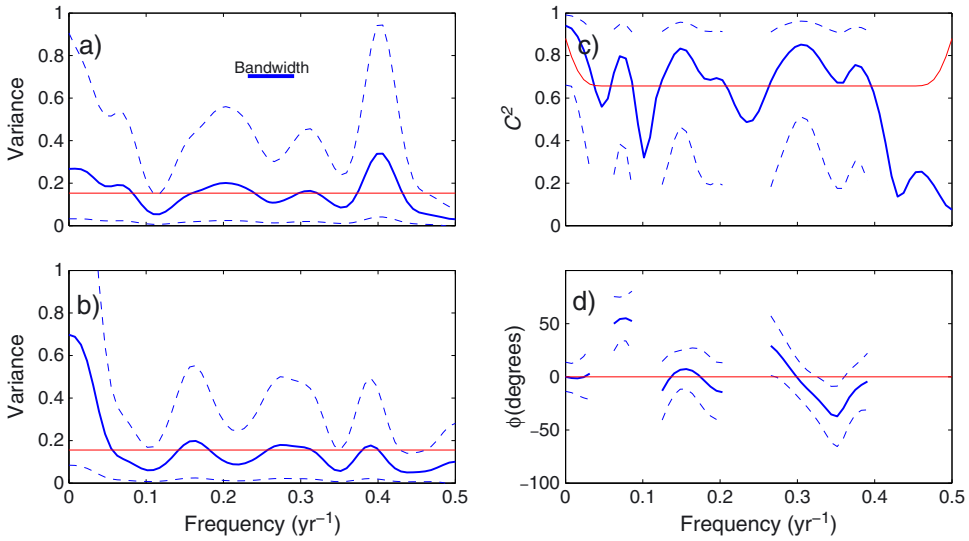

Figure 7. Frequency dependence of accuracy of reconstruction estimated from spectral and cross-spectral analysis. (a) Normalized spectrum of observed precipitation *P*. (b) Normalized spectrum of reconstructed *P*. (c) Squared coherency of observed with reconstructed *P*. (d) Phase of observed with reconstructed *P*. Analysis is on log-transformed *P*, 1946–2010. Dashed lines mark 95% confidence intervals. Red line in Figures 7a and 7b is white noise spectrum. Red line in Figure 7c marks threshold for rejection of null hypothesis of zero coherency at 95% confidence level using simplified theoretical distribution for sample squared coherency. Confidence intervals on coherency and phase ill-determined if coherency does not exceed this limit (see section 3).

recent decade contains the driest single reconstructed year, 2007. No strong regular cycles are evident in the time series plot. Low-frequency (multidecadal) features wax and wane in importance but are at times absent (e.g., 1800–1870).

[36] As already mentioned, uncertainty of reconstruction is amplified in wet years. The amplification is illustrated in a zoomed part of the reconstruction in the 1740s–1750s containing dry years and wet years (Figure 9). The 50% interval for wet year 1749 (540–865 mm) is more than 4 times as the interval for dry year 1752 (113–180 mm). This effect statistically reflects the use of log-transformed *P* as the predictand in the regression models. The confidence interval also varies slightly over time with changes in applicable nested reconstruction model. Because of the way the confidence interval is estimated (see section 3), its width is proportional to the standard deviation of cross-validation residuals for the nested model, which is about 3% larger for model M1996 than for model M1848 (Table 1).

[37] The uncertainty summarized by the confidence interval in Figure 8 should caution the user against overinterpreting small differences in reconstructed *P* from one year to another. Year 2007 is exceptional in the long-term record for being the driest reconstructed year, the lowest earlywood-width index in the standard site chronology (Table S4 in the supporting information), and for having a missing ring (lack of any growth along the sampled radii) in 69% (37 of 53) of the cores of *A. concolor* (Table S5 in the supporting information). The next highest percentage of missing rings is 43%, in 1752. But in the observed record of *P* at the key grid point, 2007 ranks as just the fourth driest year in the interval 1946–2010; the three driest observed years are 1956, 1972, and 2002 (Table S2, supporting information). Differences in ranking of years of observed and reconstruction *P* have two main sources. First, the tree ring record is a direct measure of physiological drought but is an indirect, biologically filtered, and corrupted (by noise) version of the particular

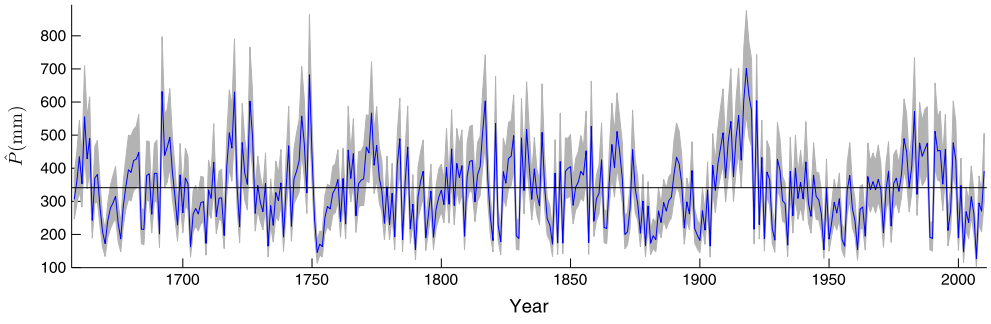

Figure 8. Time plot of reconstructed precipitation with 50% confidence interval. Horizontal line at 1946–2010 is the mean of observed precipitation.

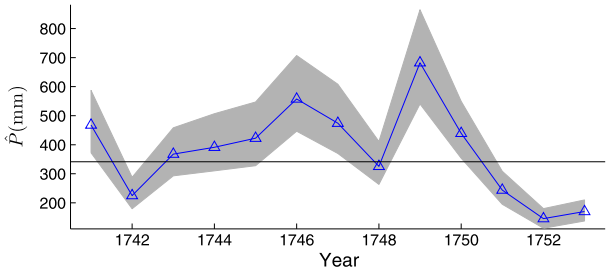

Figure 9. Zoomed portion of precipitation reconstruction with 50% confidence interval for period 1741–1753. Horizontal line at observed mean is for 1946–2010.

climatic variable (e.g., *P*) calibrated in the reconstruction model. Second, grid point observed *P* is itself an estimate, while the true *P* at the tree ring site high in the mountains of SSPM is unknown. Absolute differences in observed *P* in driest-ranking years can be so small as to be practically unimportant: For example, 11 mm separates the two driest years of the 21st century: 2002 (125 mm) and 2007 (136 mm).

[38] The high frequency of missing rings in 2007 was likely caused by extreme water stress within the trees. A survey of tree ring data over the Northern Hemisphere shows a higher frequency of occurrence where moisture is limiting to growth and a maximum occurrence in the American Southwest [*St. George et al.*, 2013]. Missing rings are also sometimes referred to as "locally absent" rings because cambial growth in even an extremely stressful year likely occurs at some point along a stem or branch of the tree [*Stokes and Smiley*, 1996, p. 14]. Early tree ring studies stressed the importance of correctly identifying missing rings to the dating of annual rings and suggested that missing-ring frequency in drought-sensitive conifers generally increases with water stress but also depends on other factors, including coring height, coring position relative to ground slope, and biological age of the ring [*Schulman*, 1956; *Fritts et al.*, 1965]. The location of 2007 toward the outer edge of most of our cores (high cambial age) would favor a higher-than-normal percentage of missing rings.

[39] Extremes of reconstructed drought in the calibration period can be put in a long-term perspective by time plots of smoothed reconstructed *P* with a reference baseline at the 1946–2010 low (Figure 10). The bottom plot in Figure 10 is the unsmoothed reconstruction (identical to the series plotted in Figure 8), while the plots above are reconstructed *P* smoothed with increasingly broad Gaussian filters. With smoothing to accentuate multiyear droughts, the 1946–2010 calibration period no longer contains the long-term low. For all three smoothed series, the lowest calibration period reconstructed *P* occurs in the 1950s drought. Four previous droughts reach a lower level for the 5.2 year filter, three reach a lower level for the 10.2 year filter, and one reaches a lower level for the 25 year filter (Table 2). Increasingly broad filters therefore highlight the relative severity of the 1950s drought.

[40] The all-time lows in reconstructed *P* in Figure 10 range in magnitude from 37% of normal with no smoothing to 75% of normal with 25 year smoothing (Table 3, last column). Comparison of lowest reconstructed and observed *P*, 1946–2010, shows that the reconstruction is conservative (reconstructed anomalies smaller than observed anomalies) for the annual values and 5.2 year smoothing but slightly overemphasizes the precipitation deficit at 25 year smoothing (Table 3, columns 3 and 4).

[41] Reconstructed *P* is broadly synchronous at low frequencies with other drought-related tree ring series in SSPM (Figure 11). Some agreement with the reconstructed Palmer Drought Severity Index from *Cook et al.* [2004] is expected because a total-width *A. concolor* chronology from our 1995 SSPM collection is part of that reconstruction's tree ring network. Strong synchrony with the other series in Figure 11 attests to the robustness of estimated timing and magnitude of droughts and wet periods across tree species. Examples are the major trough near 1754 and the peak near 1918.

[42] The broad high in reconstructed *P* near 1918 overlaps the early twentieth century North American pluvial,

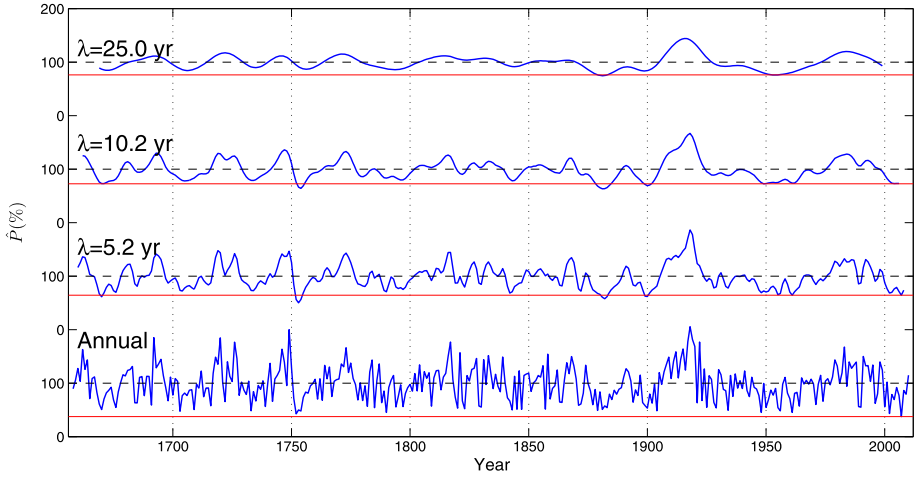

Figure 10. Time plots of annual and smoothed reconstruction. Smoothing by Gaussian filter with frequency response of 0.5 at the indicated wavelength, λ (see methods). Units for plots are percentage of normal, defined as the observed mean (341 mm) for 1946–2010, the longest calibration period of any of the time-nested models. Red horizontal reference line marks lowest reconstructed value for the 1946–2010 calibration period.

Table 2. Five Lowest Annual and Smoothed Values[a] of Reconstructed Precipitation[b], 1658–2010

	Annual		$m = 5$		$m = 9$		$m = 23$	
Rank	Year	%	Year[c]	%	Year	%	Year	%
1	2007	37.4	1753	50.1	1881	63.2	1881	74.4
2	1752	42.6	1882	57.6	1754	63.9	1953	76.2
3	2002	43.2	1670	61.4	1900	68.9	1899	83.4
4	1948	45.2	1900	62.0	1949	72.6	1706	84.2
5	1790	45.2	1961	64.3	2004	73.0	1672	84.7

[a]Local minima in Figure 10 separated by at least width of Gaussian filter (m years).
[b]As percentage of 1946–2010 observed mean (392 mm).
[c]Central year of m year smoothing.

nominally the interval 1905–1917, a period notable in the Colorado River Basin for overallocation of water resources [*Cook et al.*, 2011]. A strong early twentieth century peak in tree growth in SSPM is also evident, though less dominating, in species other than *A. concolor* (Figure 11). We speculate that the higher peak for *A. concolor* might reflect species-dependent differences in response of tree growth to moisture anomalies. *Abies concolor* is the highest-elevation species of those represented in Figure 11 and may experience heavier snowpack due to elevation or microsite differences in the sample locations. (One of our *A. concolor* subsites is 300 m higher than the sampling sites of the other species.) Moreover, differences in phenology and physiology may favor a growth response to snowpack-related moisture in one species over another. Snowmelt itself may have been anomalously slow in SSPM during the pluvial, which was apparently characterized by cool conditions in spring-summer [*Cook et al.*, 2011, Figure 4].

[43] Correlations of reconstructed *P* with other tree ring reconstructions in western North America are consistent with the spatial correlations of observed cool-season *P* mapped in Figure 3. For example, for the common period 1860–1993, reconstructed *P* is not significantly correlated with reconstructed *P* in Baja California Sur [*Diaz et al.*, 2001] or in the state of Durango, Mexico [*Cleaveland et al.*, 2003]. On the other hand, correlation is significant, though small, with cool-season *P* reconstructed from earlywood width of *Pseudotsuga menziesii* for a region centered on the border between the Mexican states of Chihuahua and Sonora [*Villanueva Díaz et al.*, 2009] and strong with a reconstruction of cool-season *P* for North American Monsoon region 2 (centered in southern Arizona) from a set of three earlywood-width tree ring chronologies in Arizona and New Mexico [*Griffin et al.*, 2013] (Table 4). Despite the significant correlation for NAM region 2, those two series differ in many important features, including an accentuated early twentieth century pluvial in SSPM and a sequence of years of large opposite-sign moisture anomalies in the early 1880s (Figure S6 in the supporting information).

[44] Data listings of the annual reconstructed *P* plotted in Figure 8, the full-length reconstructions by the individual nested models, the predictor subchronologies for nested models, the standard site chronology with time-varying sample size, and the standard indices for individual cores can be found in the supporting information. The supporting information also includes comparative time plots of the unsmoothed reconstruction in Figure 8 and the reconstruction by the least well-replicated nested model, M1658 (Figure S10).

4.3. Temperature Influence

[45] The relationship of residuals of the precipitation reconstruction with temperature, *T*, is of particular interest because increasing *T* over the southwestern United States has been associated with drought stress and reduced growth in some conifer tree species [e.g., *Williams et al.*, 2010, 2013]. If *T* were to have an important independent (of *P*) influence on earlywood width of *A. concolor* tree rings, a

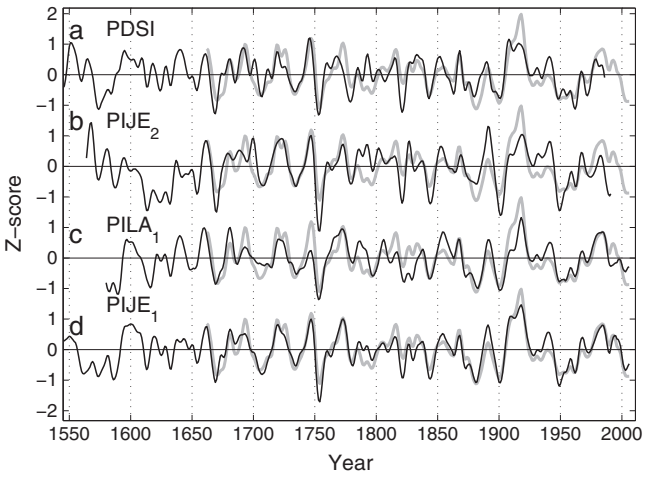

Figure 11. Smoothed Z-score time series showing consistency of reconstruction with other tree ring information for San Pedro Mártir. Gray line in all plots is the October–April precipitation reconstruction from *Abies concolor*. Black line varies as follows: (a) Palmer Drought Severity index for grid point 115°W, 30°N, from *Cook et al.* [2004], (b) International Tree Ring Data Bank Tasajera *Pinus jeffreyi* total-width chronology, developed by Franco Biondi, (c) *P. Lambertiana* earlywood-width chronology from North America Monsoon (NAM) project, (d) *P. jeffreyi* earlywood-width chronology from NAM project. Site location b within 10 km of the *Abies c.* is used in reconstruction. Site locations c and d are identical to the lower subsite of *A. concolor* collection. Smoothing by nine-weight Gaussian filter with 50% response at 10.2 years (see section 3) after conversion of annual series to Z-scores using means and standard deviations is for common period 1658–1990.

Table 3. Lowest Annual Precipitation for Various Levels of Smoothing[a]

Smoothing[b]		Observed	Reconstructed		
N	λ	1946–2010	1946–2010	1896–2010	1658–2010
1	1.0	33	37	37	37
5	5.2	56	64	62	50
9	10.2	73	73	69	63
23	25.0	82	76	76	74

[a]Units in columns 4–6 are percentage of 1946–2010 observed mean (392 mm).
[b]Number of weights (N) in Gaussian filter and wavelength (λ) in years at which frequency response of filter is 0.5 (N = 1 indicates annual, or unsmoothed, series).

drought index combining influence of P and T (e.g., Palmer Drought Severity Index) might be preferred to P as a reconstruction predictand. Moreover, earlywood-width variations would have an ambiguous interpretation, as they could be driven by T or P.

[46] The `seascorr` partial correlations (Figure 4, bottom) indicate that T for any particular month or season has no significant influence on earlywood-width independent of the influence of P in the same month or season. A more general test for independent T influence is correlation of the reconstruction residuals (observed minus reconstructed P) with seasonal-average T. Positive correlation would be consistent with high T driving reduction in tree growth below the level expected for a given anomaly in P. Because temperature-related drought stress is most likely in the warm season, when evapotranspiration is high, the correlation was computed using T averaged over the six warmest months, May–October. The regression residuals,1946–2010, are not significantly correlated with warm-season T defined in this way (($r = 0.14, N = 65, p = 0.25$).

[47] A temperature signal in earlywood width restricted to low frequencies could possibly be overlooked by the preceding correlation analysis. Warm-season-average T as defined above at the key grid point has increased over the past century. Regression of T on time for two different analysis periods yields the following estimated linear trends:

Warm season, 1897–2010: 0.86 °C/100 year
Warm season, 1946–2010: 1.52 °C/100 year

[48] Trend for both of these periods is significant ($p < 0.05$). In contrast, the reconstruction residuals have no linear trend over the period 1946–2010 ($r = 0.01, N = 65, p = 0.93$). While a drought-related temperature influence of T on tree growth at moisture-limited sites is expected, results presented in this section suggest that for *A. concolor* in SSPM such influence is effectively accounted for by covariation of temperature and precipitation.

Table 4. Correlation[a] of SSPM Precipitation Reconstruction With Other Precipitation Reconstructions

Reconstruction[b]	r	N[c]	p[d]
Baja Calif. Sur	0.14	118	0.13
Durango	0.09	134	0.32
Chihuahua/Sonora	0.26	134	0.003
NAM Region 2	0.58	71	< 0.001

[a]Product-moment correlation for period, 1860–1993, in common to the four reconstructions).
[b]Reconstructions and sources identified in text).
[c]Sample length (years) adjusted as needed for lag-1 autocorrelation of individual series (see text).
[d]p-value testing significance of correlation r.

4.4. Circulation

[49] Large-scale ocean-atmosphere influence on precipitation and tree growth in SSPM is reflected in the association of observed and reconstructed P with the Niño3.4 index, the Pacific/North America (PNA) pattern, and the Tropical/ Northern Hemisphere (TNH) pattern (Figure 12), all of which have previously been linked to Baja California precipitation anomalies [*Minnich et al.*, 2000; *Cavazos and Rivas*, 2004]. Anomalies in P are most strongly linked to Niño3.4. Some association of wet or dry years with the other two indices is also indicated but is difficult to judge because of significant correlation of Niño3.4 with the PNA pattern ($r = 0.52, N = 62, p < 0.01$) and the TNH pattern ($r = –0.34, N = 62, p < 0.01$). Comparison of the plots on the left-hand and right-hand sides of Figure 12 shows that the reconstruc-

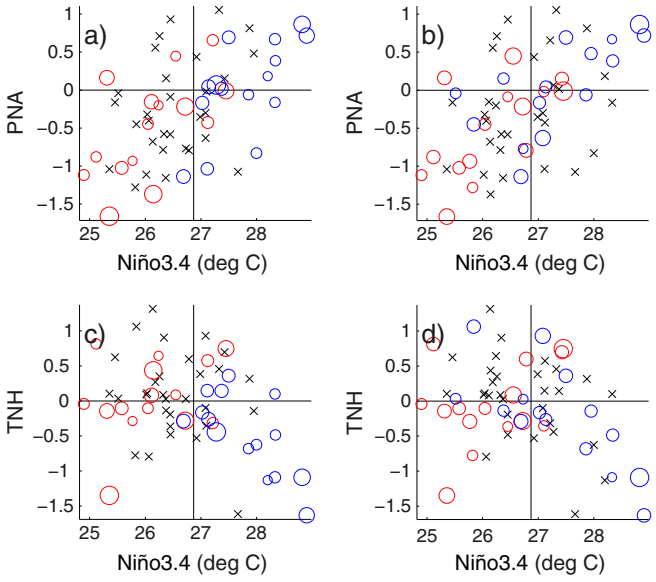

Figure 12. Association of wet and dry years in Sierra San Pedro Mártir with climatic indices. Each plot is a scatter of one index on another with points color coded and sized for cool-season (October–April) precipitation (P) anomaly. (a) Scatter of Pacific-North America (PNA) pattern on Niño 3.4 index for observed P. (b) Same as Figure 12a but for reconstructed P. (c) Scatter of Tropical/Northern Hemisphere (TNH) pattern on Niño 3.4 index for observed P. (d) Same as Figure 12c but for reconstructed P. Analysis period is 1951–2010. Years below 0.25 quantile of P are plotted as red circles, and years above 0.75 quantile are plotted as blue circles. Remaining years plotted as "x." Circles are sized proportional to absolute difference of P and its 0.25 or 0.75 quantile for 1951–2010. PNA and Niño 3.4 are November–March averages; TNH is December–February average. Vertical line, at 26.87°C, is 1981–2010 mean of Niño 3.4 index.

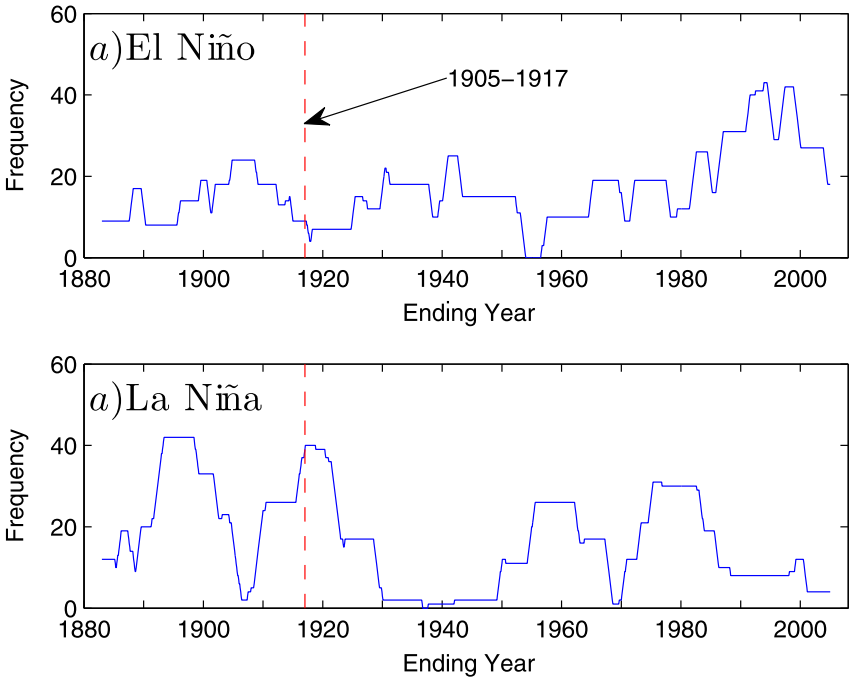

Figure 13. Early twentieth century pluvial in context of variability of Extended Multivariate ENSO index. (a) Frequency of strong El Niño bimonthly periods in 156 month (13 year) moving window. (b) Frequency of strong La Niña bimonthly periods in 156 month (13 year) moving window. Frequency is plotted at the end of 156 month period. Vertical dashed line marks the frequency for the pluvial, defined as years 1905–1917. Events delineated by highest and lowest deciles (14 values) are for the 135 year period 1871–2005.

tion effectively mirrors relationships evident in the observed *P*. Associations summarized in terms of indices in Figure 12 are consistent with composites of anomaly maps of 500 mb geopotential height and SST for subsets of the wettest and driest years at the key grid point and with distribution maps of correlation coefficients of key grid point *P* with 500 mb height and Pacific SST (see the supporting information).

[50] The importance of ENSO and North Pacific atmospheric long-wave patterns to precipitation in Baja California is discussed by *Minnich et al.* [2000]. They report that precipitation during moderate to strong El Niños is typically heavy across northern Baja California and that the anomalies tend to be greatest near 31°N (the latitude of the tree ring site) and decrease to the north and south. Heavy winter precipitation events are favored by a negative TNH pattern, with a southerly branched jet stream. Accordingly, the elevation of the snowline in SSPM may increase with increasing precipitation, such that the heaviest snowpack during negative TNH conditions is confined to the high mountains *Minnich et al.* [2000].

[51] *Minnich et al.* [2000] stress that weak-to-neutral El Niño conditions can also be accompanied by wet winters in SSPM, depending on longitudinal positioning of the Aleutian low. *Cavazos and Rivas* [2004] found that heavy precipitation events in Tijuana, about 200 km northwest of our tree ring site, on the west coast of Baja California, are favored by neutral-to-strong warm ENSO events in combination with a "neutral" PNA. The neutral PNA as defined by *Cavazos and Rivas* [2004] is characterized by a positive PNA pattern shifted southwestward such that a high occupies the Gulf of Alaska and cutoff lows and an enhanced subtropical jet bring moisture across Baja.

[52] The early twentieth century pluvial is of special interest for its prominence in the long-term reconstruction (Figure 10) as well as its broader relevance to water resources in the southwestern USA. The atmospheric circulation driving the wetness of the pluvial is as yet imperfectly understood. Tree ring records suggest that the pluvial was the signature wet event of the past 600 years in western North America and may have resulted from juxtaposition of sequential periods of favorable conditions in Northern Hemisphere circulation and in the equatorial Pacific [*Woodhouse et al.*, 2009]. By one multiproxy tabulation, the period 1897–1919 stands out in the historical record for frequent occurrences of significant El Niño activity [*Quinn and Neal*, 1992]. By the extended multivariate ENSO Index, however, a quantitative index of ENSO behavior based on anomalies SST and sea level pressure [*Wolter and Timlin*, 2011], the heart of the pluvial, 1905–1917, contains two of the six longest La Niña events and just one of the strongest El Niño events between 1871 and 1949 (http://www.esrl.noaa.gov/psd/enso/mei.ext/). Time series plots of the frequency of strong La Niña and strong El Niño months in a running 156 month, or 13 year, window also identify the pluvial as predominantly La Niña rather than El Niño (Figure 13).

[53] In a case study of the pluvial using instrumental climate data and model data, *Cook et al.* [2011] note the high frequency of years with positive Arctic Oscillation (AO+) in the interval 1905–1917. They show that the 500 hPa geopotential height anomaly associated with a composite of

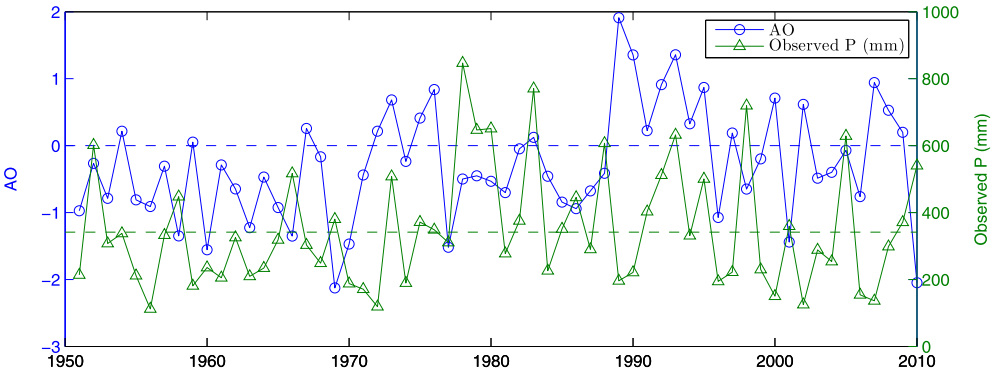

Figure 14. Time plots of Arctic Oscillation and observed cool-season precipitation at key grid point, 1951–2010. Horizontal dashed lines at neutral AO (zero) and the mean (341 mm) observed precipitation for the longest calibration period (1946–2010) of nested reconstruction models.

all AO+ years favors southwesterly transport of moisture into the Mexico and the southwestern USA and occurrence of so-called "Pineapple Express" type storms [*Dettinger*, 2004] associated with "atmospheric rivers," or narrow ribbons of concentrated tropospheric moisture delivery to the west coast of North America [e.g., *Dettinger et al.*, 2011; *Ralph and Dettinger*, 2011; *Rutz and Steenburgh*, 2012]. *Cook et al.* [2011] present this as one possible future scenario in which climate change, if accompanied by increasingly positive AO, could ameliorate climate change-related trends toward drier conditions in southwestern North America.

[54] For the recent period 1951–2010, we find that the AO (November–April average) is uncorrelated with observed P at the key grid point in SSPM ($r = –0.02$, $N = 60$, $p = 0.87$) and that the most prominent association is co-occurrence of AO+ and dry years (Figure 14). Moreover, the three most recent high-positive AO years (2000, 2002, 2007) coincide with exceptionally dry years. As implied by the near-zero correlation for the two series plotted in Figure 14, however, the AO+/dry cases are offset by other years with AO+/wet or at least by years in which an upward spike in AO coincides with an upward spike in P (e.g., 1973, 1983, 1993, 2005).

5. Conclusion

[55] The climatic signal in *A. concolor* from SSPM is demonstrated and exploited to produce an extended (1658–2010 C.E.) time series of cool-season precipitation. The reconstruction tracks observed precipitation well over the period of reliable instrumental data. The reconstruction highlights the severity, measured by size of precipitation deficit of multiyear persistent drought in the 1950s, and the magnitude of wetness of the twentieth century North American pluvial. The strong tree ring signature for the pluvial in SSPM argues for a southerly stream of moisture delivery into the southwestern USA at the time. The large-scale circulation features associated with the pluvial in SSPM remain unclear and perhaps were much different from many of the wet years in 1946–2010, when warm equatorial SST (Niño3.4) appears to be the key driving factor behind wet years. The idea that future climate change, if accompanied by a poleward shift and strengthening of the westerlies (more positive AO), might actually result in wetter winters in SSPM is plausible, as a few AO+ years have been wet in SSPM, and the pluvial may have had no strong general-circulation analog in more-recent decades. Nevertheless, such a future scenario is uncertain, as recent AO+ years have been notably dry in SSPM, and the risk is also substantial that climate change will impose increasing drought stress on the SSPM ecosystem.

[56] Tree ring data from high-elevation sites in SSPM may be well-situated for detecting storm types (e.g., Pineapple Express) delivering heavy snowpack restricted to highest elevations. More research is needed on species differences in response of tree growth to snowpack and moisture variations in general to explain why *A. concolor* has a stronger early twentieth century pluvial response than *P. jeffreyi* and *P. lambertiana* in SSPM.

[57] Any possible effect of warming on earlywood width of *A. concolor* in SSPM over the past century is yet inseparable from the effect of precipitation. Low precipitation has tended to be accompanied by high temperatures, and vice versa, such that a temperature effect on tree growth is accounted for implicitly by covariation of precipitation and temperature. It is reasonable to assume, however, that continued warming in this semiarid environment will gradually place additional drought stress on tree growth.

[58] The *A. concolor* tree ring data and precipitation reconstruction presented here are resources for improved understanding of Pacific climate and precipitation delivery to northern Mexico and the southwestern United States. The occurrence of two extremely dry years in the most recent decade, while not proving a shift in climate, may reflect drought response related to global warming. The high frequency of missing rings in *A. concolor* in the recent drought year 2007 underscores the potential vulnerability of this species in SSPM to climate change.

[59] **Acknowledgments.** This research was funded by NSF award 0823090. Tom Harlan helped with field collection in 1995 and cross-dated the 1995 samples; Mark Losleben and Brewster Malevich helped with field collections in 2010. Art Douglas provided the data set of station precipitation for Baja California.

References

Álvarez, M., R. Michel, S. Reyes-Coca, and R. Troncoso-Gaytan (2007), Pluvial precipitation in Baja California and the national astronomical observatory at San Pedro Mártir Sierra, *RevMexAA (Serie de Conferencias)*, *31*, 111–119.

Barnston, A. G., and R. E. Livezey (1987), Classification, seasonality and persistence of low-frequency atmospheric circulation patterns, *Mon. Weather Rev.*, *115*, 1083–1126.

Biondi, F., A. Gershunov, and D. R. Cayan (2001), North Pacific decadal climate variability since 1661, *J. Clim.*, *14*, 5–10.

Bloomfield, P. (2000), *Fourier Analysis of Time Series: An Introduction,* 2nd ed., 261 pp., John Wiley, New York.

Castro, C. L., H. Chang, F. Dominguez, C. Carrillo, J. Schemm, and H. H. Juang (2012), Can a regional climate model improve the ability to forecast the North American monsoon, *J. Clim.*, *25*, 8212–8237, doi:10.1175/JCLI-D-11-00441.1.

Cavazos, T., and D. Rivas (2004), Variability of extreme precipitation events in Tijuana, Mexico, *Clim. Res.*, *25*, 229–243.

Cleaveland, M. K., D. W. Stahle, M. D. Therrell, J. Villanueva-Diaz, and B. T. Burns (2003), Tree-ring reconstructed winter precipitation and tropical teleconnections in Durango, Mexico, *Clim. Change*, *59*(3), 369–388, doi:10.1023/A:1024835630188.

Conover, W. (1980), *Practical Nonparametric Statistics,* 2nd ed., 493 pp., John Wiley, New York.

Cook, B. I., R. Seager, and R. L. Miller (2011), On the causes and dynamics of the early twentieth-tentury North American pluvial, *J. Clim.*, *24*, 5043–5060, doi:10.1175/2011JCLI4201.1.

Cook, E. R. (1985), A time series approach to tree-ring standardization, PhD thesis, The University of Arizona.

Cook, E. R., and K. Peters (1981), The smoothing spline: A new approach to standardizing forest interior tree-ring width series for dendroclimatic studies, *Tree-Ring Bull.*, *41*, 45–53.

Cook, E. R., C. Woodhouse, C. M. Eakin, D. M. Meko, and D. W. Stahle (2004), Long-term aridity changes in the western United States, *Science*, *306*, 1015–1018.

Cook, E. R., R. Seager, M. A. Cane, and D. W. Stahle (2007), North American drought: Reconstructions, causes, and consequences, *Earth Sci. Rev.*, *81*, 93–134.

Dawdy, D. R., and N. C. Matalas (1964), Statistical and probability analysis of hydrologic data, part III analysis of variance, covariance and time series, in *Handbook of Applied Hydrology: A Compendium of Water-Resources Technology*, edited by V. T. Chow, pp. 8.69–8.90, McGraw-Hill Book Company, New York, 1440 pp.

Dettinger, M., (2004), Fifty-two years of Pineapple-Express storms across the west coast of North America, *Pier Project Rep., California Energy Commission Rep. CEC-500-2005-004*, U.S. Geological Survey, Scripps Institution of Oceanography, 15 pp., available online at http://www.energy.ca.gov/2005publications/CEC-500-2005-004/CEC-500-2005-004.PDF.

Dettinger, M. D., F. M. Ralph, T. Das, P. J. Neiman, and D. Cayan (2011), Atmospheric rivers, floods, and the water resources of California, *Water*, *3*, 455–478, doi:10.3390/w3020445.

Diaz, S. C., R. Touchan, and T. W. Swetnam (2001), A tree-ring reconstruction of past precipitation for Baja California Sur, Mexico, *Int. J. Climatol.*, *21*, 1007–1019, doi:10.1002/joc.664.

Diaz, S. C., M. D. Therrell, D. W. Stahle, and M. K. Cleaveland (2002), Chihuahua (Mexico) winter-spring precipitation reconstructed from tree-rings, 1647–1992, *Clim. Res.*, *22*, 237–244.

Fritts, H. C., D. G. Smith, J. W. Cardis, and C. A. Budelsky (1965), Tree-ring characteristics along a vegetation gradient in northern Arizona, *Ecology*, *46*, 394–401.

Fritts, H. C., J. Guiot, and G. A. Gordon (1990), Verification, in *Methods of Dendrochronology: Applications in the Environmental Sciences*, edited by E. R. Cook and L. A. Kairiukstis, pp. 178–185, Kluwer Academic Publishers, Dordrecht, 394 pp.

Griffin, D., D. M. Meko, R. Touchan, S. W. Leavitt, and C. A. Woodhouse (2011), Latewood chronology development for summer-moisture reconstruction in the US Southwest, *Tree Ring Res.*, *67*(2), 87–101.

Griffin, D., C. A. Woodhouse, D. M. Meko, D. W. Stahe, H. L. Faulstich, C. Carillo, R. Touchan, C. Castro, and S. Leavitt (2013), North American monsoon precipitation reconstructed from tree-ring latewood, *Geophys. Res. Lett.*, *40*, 954–958, doi:10.1002/grl.50184.

Haan, C. T. (2002), *Statistical Methods in Hydrology,* 2nd ed., 496 pp., Iowa State Press, Ames, Iowa.

Hastings, J. R., and R. M. Turner (1965), Precipitation regimes in Baja California, Mexico, *Geografiska Annaler*, *47A*(4), 204–223.

Little, E. L., Jr. (1971), Atlas of United States trees, volume 1, conifers and important hardwoods: Misc. Pub. 1146, *Tech. Rep.*, 9 pp., 200 maps, Washington, D. C.

Lu, J., G. Chen, and D. M. W. Frierson (2008), Response of the zonal mean atmospheric circulation to El Niño versus global warming, *J. Clim.*, *21*(22), 5835–5851.

Markham, C. G. (1972), Baja California's climate, *Weatherwise*, *25*, 64–76.

Meko, D. (1997), Dendroclimatic reconstruction with time varying predictor subsets of tree indices, *J. Clim.*, *10*(4), 687–696.

Meko, D. M., M. D. Therrell, C. H. Baisan, and M. K. Hughes (2001), Sacramento River flow reconstructed to A.D. 869 from tree rings, *J. Am. Water Resour. Assoc.*, *37*(4), 1029–1040.

Meko, D. M., R. Touchan, and K. A. Anchukaitis (2011), Seascorr: A MATLAB program for identifying the seasonal climate signal in an annual tree-ring time series, *Comput. Geosci.*, *37*, 1234–1241.

Meko, D. M., C. A. Woodhouse, and K. Morino (2012), Dendrochronology and links to streamflow, *J. Hydrol.*, *412–413*, 200–209.

Michaelsen, J. (1987), Cross-validation in statistical climate forecast models, *J. Clim. Appl. Meteorol.*, *26*, 1589–1600.

Minnich, R. A., E. Franco-Vizcaíno, J. Sosa-Ramírez, J. H. Burk, W. J. Barry, M. G. Barbour, and H. de la Cueva-Salcedo (1997), A land above: Protecting Baja California's Sierra San Pedro Mártir within a biosphere reserve, *J. Southwest*, *39*(3/4), 613–695.

Minnich, R. A., E. Franco-Vizcaíno, and R. J. Dezzani (2000), The El Niño/Southern Oscillation and precipitation variability in Baja California, Mexico, *Atmósfera*, *13*, 1–20.

Mitchell, J. M., Jr., B. Dzerdzeevskii, H. Flohn, W. L. Hofmeyr, H. H. Lamb, K. N. Rao, and C. C. Walln (1966), Climatic change, technical note no. 79, *Report of a Working Group of the Commission for Climatology No. 195 TP 100*, 81 pp., WMO, Geneva, Switzerland.

Mo, K. C., and R. E. Livezey (1986), Tropical-extratropical geopotential height teleconnections during the Northern Hemisphere winter, *Mon. Weather Rev.*, *114*, 2488–2515.

Ni, F., M. K. Hughes, A. C. Comrie, and G. Funkhouser (2002), Cool-season precipitation in the southwestern USA since A.D. 1000: Comparison of linear and nonlinear techniques for reconstruction, *Int. J. Climatol.*, *22*, 1645–1662.

Panofsky, H. A., and G. W. Brier (1968), *Some Applications of Statistics to Meteorology*, 224 pp., The Pennsylvania State University, University Park, Pennsylvania.

Pike, C. B., (1972), Some meteorological aspects of the seasonal distribution of precipitation in the western United States and Baja California, *Tech. Rep.*, 139 pp., University of California Water Resources Center, 139 pp.

Quinn, W. H., and V. T. Neal (1992), The historical record of El Niño events, in *Climate Since 1500*, edited by R. S. Bradley, and P. D. Jones, pp. 623–648, Routledge, London and New York, 706 pp.

Ralph, F. M., and M. D. Dettinger (2011), Storms, floods, and the science of atmospheric rivers, *Eos Trans. AGU, 92*, 265–266, doi:10.1029/2011EO320001.

Rutz, J. J., and W. J. Steenburgh (2012), Quantifying the role of atmospheric rivers in the interior western United States, *Atmos. Sci. Lett.*, *13*, 257–261, doi:10.1002/asl.392.

Salzer, M. W., and K. F. Kipfmueller (2005), Reconstructed temperature and precipitation on a millennial timescale from tree-rings in the southern Colorado Plateau, USA, *Clim. Change*, *70*, 467–487.

Schulman, E. S. (1956), *Dendroclimatic Changes in Semiarid America*, 142 pp., Univ. of Ariz. Press, Tucson, Ariz.

Shindell, D. T., R. L. Miller, G. A. Schidt, and L. Pandalfo (1999), Simulation of recent northern winter climate trends by greenhouse-gas forcing, *Nature*, *399*, 452–455.

St. George, S., T. R. Ault, and M. C. A. Torbenson (2013), The rarity of absent growth rings in Northern Hemisphere forests outside the American Southwest, *Geophys. Res. Lett.*, *40*, 3727–3731, doi:10.1002/grl.50743.

Stockton, C. W., and D. M. Meko (1983), Drought recurrence in the Great Plains as reconstructed from long-term tree-ring records, *J. Clim. Appl. Meteorol.*, *22*, 17–29.

Stokes, M. A., and T. L. Smiley (1996), *An Introduction to Tree-Ring Dating*, 73 pp., Univ. of Ariz. Press, Tucson. (originally published 1968, University of Chicago Press).

Thompson, D. W. J., and J. M. Wallace (1998), The Arctic Oscillation signature in the wintertime geopotential height and temperature fields, *Geophys. Res. Lett.*, *25*, 1297–1300.

Touchan, R., D. M. Meko, and M. K. Hughes (1999), A 396-year reconstruction of precipitation in southern Jordan, *J. Am. Water Resour. Assoc.*, *35*, 45–55.

Touchan, R., C. A. Woodhouse, D. M. Meko, and C. Allen (2011), Millennial precipitation reconstruction for the Jemez Mountains, New Mexico, reveals changing drought signal, *Int. J. Climatol.*, *31*(6), 896–906.

Villanueva Díaz, J., P. Z. Fulé, J. Cerano Paredes, J. Estrada Ávalos, and I. Sánchez Cohen (2009), Reconstrucción de la precipitación estacional para el barlovento de la Sierra Madre Occidental con anillos de crecimiento de Pseudotsuga menziesii (Mirb.) Franco, *Rev. Ciencia Forestal in México*, *34*(105), 39–71.

Weisberg, S. (1985), *Applied Linear Regression,* 2nd ed., 324 pp., John Wiley, New York.

Wigley, T. M. L., K. R. Briffa, and P. D. Jones (1984), On the average value of correlated time series, with applications in dendroclimatology and hydrometeorology, *J. Clim. Appl. Meteorol.*, *23*, 201–213.

Wilks, D. S. (1995), *Statistical Methods in the Atmospheric Sciences, International Geophysics Series,* vol. 59, 467 pp., Academic Press, San Diego.

Williams, A. P., C. D. Allen, C. I. Millar, T. W. Swetnam, J. Michaelsen, C. J. Still, and S. W. Leavitt (2010), Forest responses to increasing aridity and warmth in the southwestern United States, *PNAS*, *107*(50), 21,289–21,294.

Williams, A. P., et al. (2013), Temperature as a potent driver of regional forest drought stress and tree mortality, *Nature Clim. Change*, *3*(3), 292–297.

Willmott, C. J., and K. Matsuura (1995), Smart interpolation of annually averaged air temperature in the United States, *J. Appl. Meteorol.*, *34*, 2577–2586.

Willmott, C. J., and S. M. Robeson (1995), Climatologically aided interpolation (CAI) of terrestrial air temperature, *J. Appl. Climatol.*, *15*(2), 221–228.

Wolter, K., and M. S. Timlin (2011), El Niño/Southern Oscillation behaviour since 1871 as diagnosed in an extended multivariate ENSO index (MEI.ext), *Int. J. Climatol.*, *31*(7), 1074–1097.

Woodhouse, C. A., J. L. Russell, and E. R. Cook (2009), Two modes of North American drought from instrumental and paleoclimatic data, *J. Clim.*, *22*, 4336–4347, doi:10.1175/2009JCLI2705.1.